



# Quality monitoring for a resistance spot weld process of galvanized dual-phase steel based on the electrode displacement

M. Ullrich<sup>1</sup> · M. Wohner<sup>1</sup> · S. Jüttner<sup>1</sup>

Received: 18 September 2023 / Accepted: 8 February 2024  
© The Author(s) 2024

## Abstract

In previous works, it has been found out that the electrode displacement in resistance spot welding has a high potential to be used as a measurement factor to monitor joint quality and to subsequently optimize the welding parameters. By extracting characteristic points in the displacement curve, it is possible to create and evaluate different parameter sets and to predict the formation of expulsion. These characteristic points include for example the maximum displacement of the electrodes, the time of the maximum displacement, the indentation displacement in the weld and hold time, or the velocity of the electrodes. In previous work, it was already shown that the indentation displacement showed satisfying results in predicting the nugget diameter for a press hardened 22MnB5 + AS150 under laboratory conditions. Based on that, a newly derived methodology for using the electrode displacement in monitoring a resistance spot weld process is shown for a galvanized dual-phase steel CR440Y780T-DP GI50/50-U. This methodology combines the knowledge of previous research and is split into three steps: the detection of manufacturing discontinuities, the evaluation of expulsion, and the monitoring of the nugget diameter. For this, the electrode velocity at the beginning of the process and the indentation displacements in the weld and hold time are being used to evaluate the resistance spot welding process.

**Keywords** Resistance spot welding · Electrode displacement · Data analysis · Process monitoring · Quality assurance

## 1 Introduction

Resistance spot welding (RSW) is the dominant welding process in automotive body production. A modern car body has up to 6000 spot welds, where sheets with different thicknesses, chemical compositions, mechanical properties, and coatings are joined. This leads to new challenges, such as the joining of asymmetrical multi-sheet joints, where the wrong choice of parameters can result in a missing connection of the thin outer sheet. Furthermore, unavoidable disturbance variables such as gaps, misalignments, and adhesive in the joining area occur during production, which further reduce process stability. For this reason, it is necessary to select the

welding current, welding time and electrode force parameters in accordance with the joining task in order to ensure adequate process stability. The choice of suitable parameters is made on the basis of the user's experience or with a high level of experimental effort, whereby disturbances can shift this process window and render it invalid [1].

## 2 State of the art

### 2.1 Electrode displacement in resistance spot welding

Resistance spot welding is based on the formation of a welding nugget between two or more electrically conductive components under the effect of a locally applied electric current. A force is exerted with the aid of the electrodes placed on both sides, whereby these simultaneously form the starting point of the current flow [2, 3]. Figure 1 shows a simulated resistance spot weld, made in *SORPAS*® 2D, for a two sheet stack-up of galvanized steel. The force applied in this process is referred to as the electrode force  $F_E$ , the electric current introduced into

---

Recommended for publication by Commission III—Resistance Welding, Solid State Welding, and Allied Joining Process.

---

✉ M. Ullrich  
moritz.ullrich@ovgu.de

<sup>1</sup> Institute for Materials and Joining Technology, Otto-von-Guericke University Magdeburg, 39106 Magdeburg, Germany

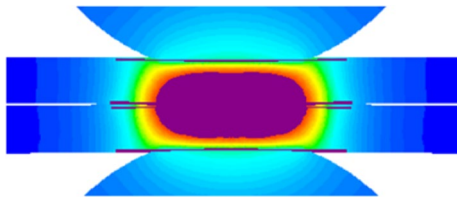


**Fig. 1** Simulation of a resistance spot weld (created in *SORPAS® 2D*)

the joining partners (resulting from the welding voltage  $U_w$ ) as the welding current  $I_w$ , and the time during which the welding current is present as the welding time  $t_w$ , according to ISO 17677-1:2022-02. In addition to that, the process is extended by a squeeze time  $t_s$  and hold time  $t_h$  to ensure sufficient force buildup and nugget solidification [3].

In this context, weld nugget formation can be described according to Gedeon et al. based on the electrode displacement signal and divided into six stages [4]. Figure 2 shows an exemplary curve of the electrode displacement of a resistance spot weld, plotted over time, and the five stages of weld nugget formation for galvanized steel sheets.

The stages of the electrode displacement can be described as shown in Table 1 [4].

A potential sixth phase can be seen under the influence of expulsion, where there is a sharp drop in the electrode displacement (Fig. 2). After the welding current is shut off at the end of phase five, the electrode force is kept up in the hold time to cool the produced joint. During this hold time, the electrodes sink further into the material.

The timing and quantitative characteristics of the phases depend, among other phenomenon, on the process parameters electrode force and welding current, on the material combination and coating, and on production-related disturbances. It is also possible to describe the nugget formation via the dynamic resistance; however, the electrode

**Table 1** Stages of the electrode displacement acc. to [4]

Phase	Description
1:	Build-up of the electrode force, flattening of asperities
2:	Thermal expansion of the coating
3:	Melting of the coating
4:	Thermal expansion of the substrate
5:	Melting of the substrate

displacement proved to more sensitive to changes of the boundary conditions and independent from the current generation [5–7] (Fig. 3).

## 2.2 RSW of galvanized dual-phase steels

Dual-phase steels offer beneficial properties in automotive manufacturing by combining high strength and energy absorption with good ductility and formability. This can be realized by a controlled heat treatment during the steel production, which produces a composite of a ferritic matrix with a set fraction of martensitic phase [8, 9].

In the automotive use, dual-phase steels are generally galvanized to protect the material against corrosion. The thickness of the zinc layer influences the resistance spot welding process by shifting the minimal welding current to higher values and narrowing the process window with increasing coating thickness [10, 11]. Especially high-grade dual-phase steels, i.e., third generation advanced high strength steels (AHSS) like TRIP1180 or DP1180, can experience significant loss of strength due to liquid metal embrittlement (LME) caused by the coating. However, this phenomenon does not seem to have a significant impact on lower grade dual-phase steels like DP780 [12, 13].

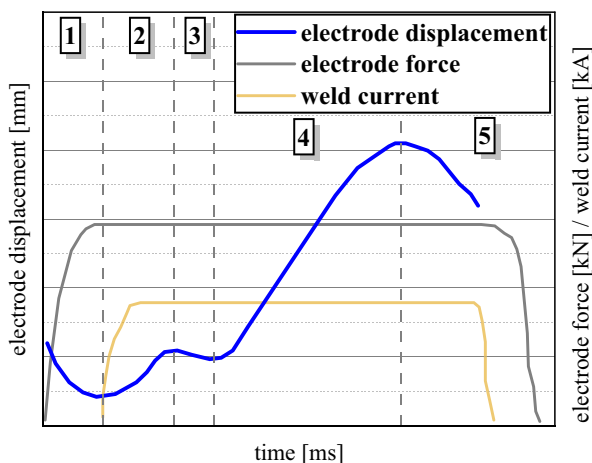


**Fig. 2** Qualitative electrode displacement for a galvanized steel, based on [4]

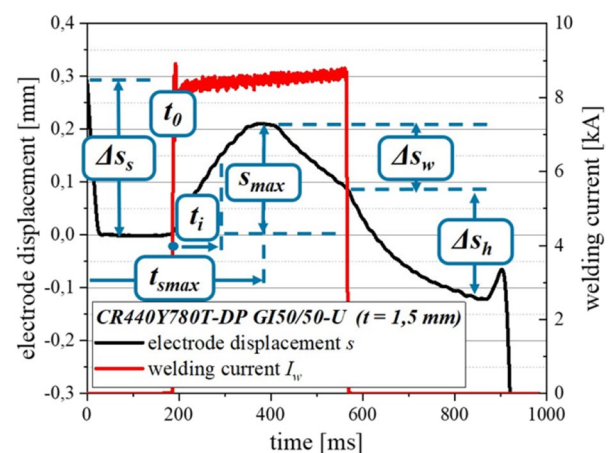


**Fig. 3** Electrode displacement with the investigated characteristic values

The heat input during the resistance spot welding process causes a characteristic softened zone (*HAZ*), which effects the failure mode and overall strength of the joint. Particularly high differences between the hardness in the joint and the heat affected zone can lead to an unwanted interfacial failure. However, it has been found out by Nayak et al. that this *HAZ*-softening is more pronounced in DP980 compared to a DP780 [8]. In terms of the quality assessment based on the electrode displacement, there can be no specific conclusion drawn from the current literature. It is however expected that there will be no significant differences compared to other galvanized steel grades.

### 3 Experimental setup and procedures

#### 3.1 General approach

The test sequence is divided into three main components. The first component consists of the determination of a suitable welding area based on SEP 1220–2:2011–08. This is followed by the analysis of the process data recorded during the determination of the welding area. In the third step, this data is correlated with the welding quality. Subsequently, the parameters are to be adjusted based on the knowledge gained from the process data analysis.

The characteristic values used in the investigations are based on the research by Wohner et al. [1] and Zhang et al. [14].

The focus was thereby laid on the following characteristic values:

$\Delta s_s$  = indentation displacement in the squeeze time.

$s_{max}$  = maximum displacement.

$t_{smax}$  = time of the maximum displacement.

$\Delta s_w$  = indentation displacement in the weld time.

$\Delta s_h$  = indentation displacement in the hold time.

$v_i$  = average nugget growth velocity at the time  $t_i$ .

The values are calculated as follows:

$$\Delta s_s = s_0 - s_{t_0} \quad (1)$$

$$\Delta s_w = s_{max} - s_{t_{w,end}} \quad (2)$$

$$\Delta s_h = s_{t_{w,end}} - s_{t_{h,end}} \quad (3)$$

$$v_i = \frac{s(t_i) - s(t_0)}{t_i - t_0} \quad (4)$$

where the variables can be defined as:

$s_0$  = electrode displacement at the start of the squeeze time.

$s_{t_0}$  = electrode displacement at the start of the weld time.

$s_{w; end}$  = electrode displacement at the end of the weld time.

$s_{h; end}$  = electrode displacement at the end of the hold time.

$t_0$  = start of welding current.

#### 3.2 Welding equipment and material

The tests shown were carried out on a C-frame spot weld system (*NIMAK GmbH*) with an electromagnetic force generation system (*magneticDRIVE®*). The current generation and control are carried out by a 1 kHz medium frequency DC inverter (*Bosch AG*). Additional selected experiments were carried out on a pneumatic C-frame (*Harms & Wende GmbH & Co. KG*) and an electromagnetically operated C-clamp (*NIMAK GmbH*) to analyze the transferability of the obtained knowledge. However, the focus of this paper is on the developed methodology based on the results of the *magneticDRIVE®* C-frame system (*NIMAK GmbH*).

The two electrode tips used in the investigation are a F1-16–20-50–6 and a B0-16–20-50–6-36 shape. The selection was made according to ISO 5821:2010–04. The investigated material is a galvanized CR440Y780T-DP GI50/50-U, according to VDA 239–100:2016–05. The sheet thickness is  $t = 1.5$  mm with a specimen size of  $l \times b = 45 \text{ mm} \times 45 \text{ mm}$  in accordance with the SEP 1220–2:2011–08. The machine settings, mechanical properties and chemical composition of the investigated material can be found in Tables 2 and 3. The chemical composition was determined by atomic emission spectroscopy (*AES*). The initial condition is taken with an electrode force of  $F_E = 4.5$  kN and shown F1-16–20-50–6 electrode tips.

#### 3.3 Variation of the boundary conditions

A variety of common manufacturing discontinuities have been investigated to simulate possible scenarios in the automotive car body manufacturing [2]. An overview of the investigated discontinuities is given in Table 4.

The force and electrode variation, in addition to the disturbance analysis, are used to investigate the influence of production-related discontinuities and the effects of different electrode shapes and electrode forces on the characteristic displacement values. For this purpose, a welding range was identified in accordance to SEP 1220–2:2011–08 with the different boundary conditions. The welding ranges were then compared to each other.

The comparison was made with regard to the size of the weld area and the nugget geometry, as well as with regard to the recorded process data. The disturbance analysis was performed with the same parameters as the initial state with

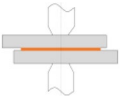
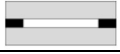
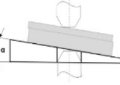
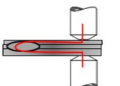
**Table 2** Selected welding parameters and machine setting

Squeeze time [ms]	Weld time [ms]	Hold time [ms]	Electrode force [kN]	Force generation	Cooling	Electrode shape (acc. to ISO 5821:2010-04)
200	380	300	3.5–5.5	Electromagnetic	11 l/min 14.5 °C	F1-16–20-8–50-6 B0-16–20-50–6-36

**Table 3** Mechanical properties and chemical composition of the investigated material

Yield strength (min.) [MPa]	Tensile strength (min.) [MPa]	Alloy element (wt. %)									
		C	Si	Mn	P	S	Al	Cu	B	Ti+Nb	Cr+Mo
440	780	0.127	0.166	1.915	0.015	0.004	0.041	0.009	0.001	0.004	0.224

**Table 4** Investigated discontinuities

Discontinuity	Used design	
Adhesive	Betamate 1640	
Gap	1.0 mm and 2.0 mm	
Angular misalignment	3° and 5°	
Shunting	12.0 mm and 15.0 mm	

an electrode force of  $F_E = 4.5 \text{ kN}$  and electrode tips of the shape F1-16–20-50–6 (acc. to ISO 5821:2010–04).

For the investigation of the adhesive, gap, and angular misalignment, 45 mm × 45 mm specimens have been used. To investigate the shunting effect, bigger specimens with the size of 45 mm × 90 mm were required.

The gap was inserted by two electrically isolated spacers with an inner distance of 35 mm to each other and a thickness according to the investigated gap height. The adhesive was manually applied in a linear form across the center of the specimen with a length of 45 mm and width of 5 mm. After welding, the adhesive was hardened with a temperature of 180 °C for 30 min. To simulate angular misalignment, an electrically isolated insert was used, in which the specimens were fixated.

### 3.4 Parameter selection

Up to now, it is necessary to specifically train each material combination for each parameter variation on existing plant systems in industrial use [15, 16]. In order to minimize this high experimental effort, a methodology is being developed

to monitor the weld quality non-destructively and to simplify the established welding range determination.

In the first step of the investigations, a database is created for the model to be developed for the interpretation and analysis of the electrode movement. For this purpose, welding ranges are determined for CR440Y780T-DP GI50/50-U dual-phase steel according to SEP 1220–2:2011–08, while the process signals are recorded for each weld. The welding ranges are then recorded again under the influence of different electrode forces, tip geometries, and manufacturing discontinuities and compared with the initial state.

### 3.5 Data analysis for evaluation of weld quality

The time-synchronous recording and subsequent analysis of the process data, using an appropriate methodology, enable the quality monitoring and adaptive control of the resistance spot welding process, while this paper focuses on the quality assessment. In order to realize this, appropriate process variables, which can reflect the nugget development, are necessary. These mechanical and electrical values are shown in Table 5. All were recorded in the shown investigation.

In addition to the measured values recorded in the process, it is possible to calculate further process variables from these.

These are, for example, the electrical resistance, the energy input, and the velocities of the electrodes calculated from the measured displacement. It should be noted that the given Formulas 5 and 6 are only valid for direct current (DC).

$$R = \frac{U_w}{I_w} \quad (5)$$

$$P = U_w * I_w \quad (6)$$

Experiments carried out beforehand and the relevant literature have already shown that the electrode displacement

**Table 5** Recorded mechanical and electrical values, based on [1]

Mechanical values	Electrical values
<ul style="list-style-type: none"> <li>• Electrode force <math>F_E</math> [kN]</li> <li>• Electrode displacement <math>s</math> [<math>\mu\text{m}</math>; mm]</li> </ul>	<ul style="list-style-type: none"> <li>• Electric (welding) voltage <math>U_w</math> [mV]</li> <li>• Electric (welding) current <math>I_w</math> [kA]</li> </ul>

can reliably reflect the nugget development [1, 17, 18]. In addition to that, external influences such as a change in the material combination, the formation of expulsion, and the production-related discontinuities can be detected with the aid of the electrode displacement. A newly developed methodology is to be used for non-destructive quality monitoring and parameter adjustment in the resistance spot welding process.

In the context of the experiments shown here, the data was collected as follows:

- Electric current via a Rogowski belt MB-400 K (*Amada Miyachi Corporation*)
- Electric voltage via direct connection to the electrodes
- Electrode force via a piezoelectric force platform
- Electrode displacement via an absolute displacement sensor GT2-H12 (*Keyence Corp.*)

The data was recorded in a Weldanalyst-S3 (*HKS Prozesstechnik GmbH*) with a sampling frequency of up to 23.6 kHz and forwarded to a computer in a readable format. Because of the sensor limitation, the electrode displacement is recorded with a sampling rate of 1 kHz. The schematic measurement setup is illustrated in Fig. 4.

### 3.6 Evaluation of expulsion intensity

To evaluate the intensity of expulsion, the welding specimen (45 mm  $\times$  45 mm) were, according to Xia et al. [19], weighed before and after welding with a precision scale Satorius CP64 (*Satorius AG*). The systematic deviation is  $\pm 0.1$  mg. The loss of mass  $\Delta M$  was calculated as follows:

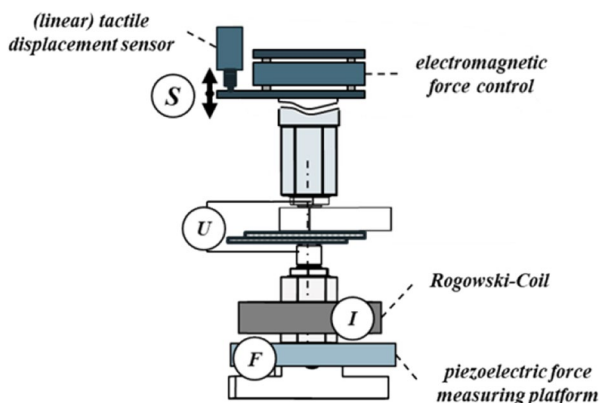


**Fig. 4** Data acquisition on the used spot weld machine

$$\Delta M = m_{\text{prewelding}} - m_{\text{postwelding}} \quad (7)$$

The sensitivity of the methodology was verified by welding at the upper limit of the welding range without expulsion. The loss of weight was calculated at  $\Delta M \approx 0.005$  g, which was expected to resemble the vaporized zinc coating. Tests were carried out beforehand to determine the amount of expelled material stuck on the weld material. For this, the specimens were weighed, opened by chisel testing, the visible material removed and weighed again (acc. to Xia et al. [19]). As there was no significant difference visible in the weight difference with and without the removal of expelled material at the faying interface for the investigated material, it was decided to use the weight right after welding. To weigh the influence of process parameters on the expulsion intensity, a design of experiment (*DoE*) has been carried out, based on the upper limit of the welding range. In a *face-centered response surface design*, the electrode force was varied by  $F_E \pm 1$  kN, the welding time was varied by  $t_w \pm 100$  ms, and the welding current was increased to up to 2 kA above the upper limit of the welding range.

## 4 Results

### 4.1 Monitoring of a resistance spot weld process

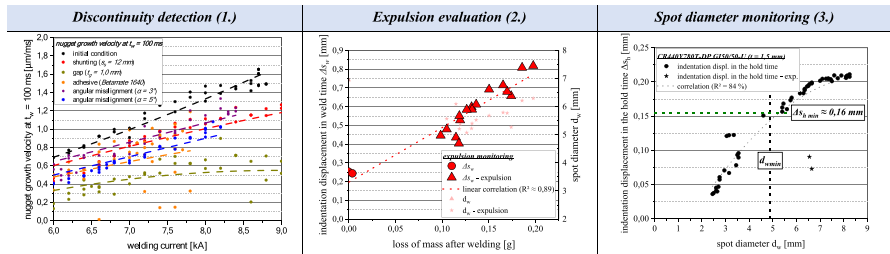
For a resistance spot weld of CR440Y780T-DP GI50/50-U ( $t = 1.5$  mm), it will be shown by way of example how the electrode displacement can be used to detect a manufacturing discontinuity, evaluate expulsion, and determine the weld quality. Figure 5 shows the following:

- (1) The comparison of the nugget growth velocity in the initial state (black) and under the influence of the investigated manufacturing discontinuities
- (2) The evaluation of occurring expulsion based on the indentation displacement within the welding time ( $\Delta s_w$ ; red), represented via the loss of mass.
- (3) Quality assessment by monitoring the spot diameter based on the indentation displacement within the hold time ( $\Delta s_h$ )

Figure 5(1) clearly shows that the nugget growth velocity at the time  $t_w = 100$  ms shifts to lower values with increasing welding current under the influence of different manufacturing discontinuities. This enables the determination of a



**Fig. 5** Evaluation of a resistance spot weld process based on the electrode displacement



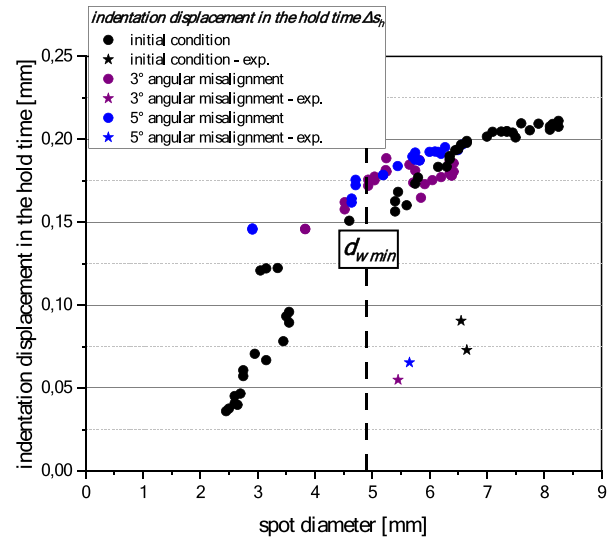
corresponding curve as a function of the welding current. The trend has shown to be transferable to the other disturbance variables investigated (cf. Table 4), with the velocities being shifted downward according to the variable being investigated. There can also be a trend derived for the common angular misalignment, where the nugget growth velocity is shifted downward based on its intensity. The finding that the average nugget growth velocity was lowered for all disturbances in comparison to the initial state makes it possible to detect an unwanted circumstance in the first half of the resistance spot welding process. However, it is not possible to differentiate the disturbances clearly from each other.

Figure 5(2) shows, following Xia et al. [19], the potential for using the indentation displacement in the weld time. For this purpose, the joining partners were weighed with a precision scale before welding, welded and then weighed again (cf. Section 3.6). The welding parameters were varied with the aid of a design of experiment (DoE) in order to be able to evaluate the influence of these on the expulsion intensity. The loss of mass shows a clear linear correlation with the respective indentation displacement within the welding time ( $\Delta s_w$ ) of  $R^2 \approx 98\%$ . A critical indentation displacement could not be generated with regard to the spot diameter.

Following the welding process, as shown in Fig. 5(3), the indentation displacement in the holding time ( $\Delta s_h$ ) can be used to monitor the spot diameter. Here, for the shown combination of CR440Y780T-DP GI50/50-U ( $t = 1.5$  mm), it would be necessary to achieve a value of  $\Delta s_{h\ min} \geq 0.16$  mm.

Furthermore, the characteristic value proves to be resilient to occurring disturbance variables, in particular an angular misalignment, which is common in the automotive car body production. The indentation displacement over the measured spot diameter can be seen in Fig. 6, where the minimal necessary indentation displacement in the hold time is approx.  $\Delta s_{h\ min} \geq 0.175$  mm for both 3° and 5° angular misalignment.

In addition to that, Fig. 7 shows the indentation displacement in the hold time for the other investigated manufacturing discontinuities (cf. Table 4 and Fig. 5). Here, it can be seen that especially the shunting ( $s_s = 12$  mm) and gap ( $t_g = 1.0$  mm) lead to higher spot diameters at similar indentation displacements. The adhesive affects the correlation only slightly.



**Fig. 6** Indentation displacement in the hold time in the initial condition and under angular misalignment

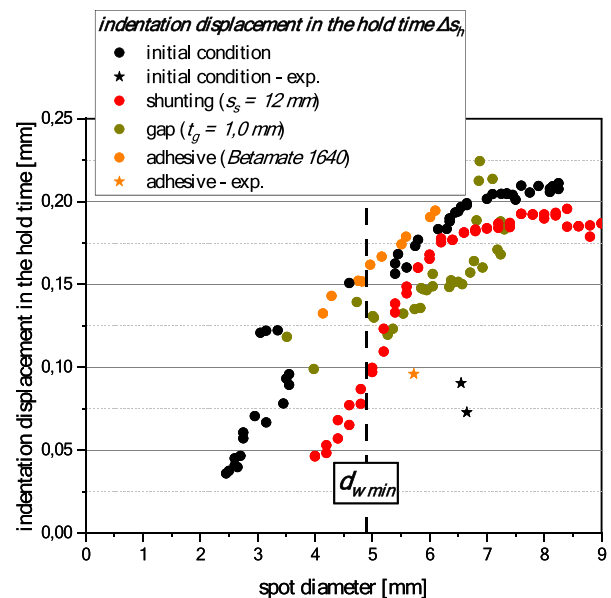


**Fig. 7** Indentation displacement in the hold time in the initial condition and under the influence of shunting, gap, and adhesive

### 4.2 Derived methodology for using the electrode displacement

Based on the previous findings, a methodology has been derived which should enable the evaluation of a resistance spot welding process based on the electrode displacement, as shown in Fig. 8.

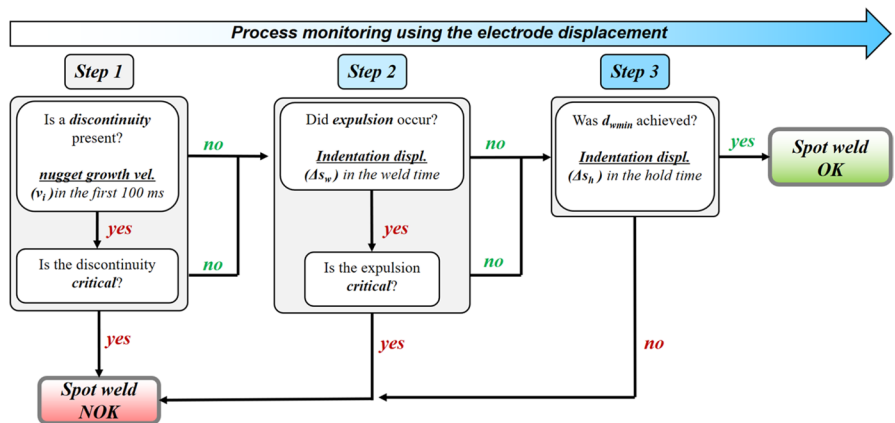
Various characteristic values in the electrode displacement are to be used to enable the quality monitoring. The analysis is divided into three steps (cf. Figure 8):

- (1) The detection of a present discontinuity based on the nugget growth velocity at the time  $t_i$  (linear)
- (2) The detection and evaluation of expulsion based on the indentation displacement in the weld time  $\Delta s_w$
- (3) The evaluation of the present spot diameter based on the indentation displacement in the hold time  $\Delta s_h$

The calculations can be extracted from Sect. 3.1.

First of all, it should be determined whether a production-related discontinuity is present in the process and, if so, whether this exceeds a critical level. If a critical dimension is exceeded, which is reflected in the lowered or raised rate of growth velocity, the process should be stopped and the disturbance corrected accordingly. In addition to the elimination of the cause of the fault, the reason for the abort is that it can be seen that the characteristic values lose their validity when a critical disturbance variable is exceeded. The specific critical value has to be determined for the required application, the material used, and the spot welding apparatus. The use of the characteristic value is not recommended in this case. It is expected, that the average nugget growth velocity, especially in the first half of the process, represents the present current density. Consequently, if a discontinuity is present, the current density and the electrode displacement signal are altered significantly. If it is determined that no critical disturbance variable is present, the analysis proceeds to step two.

Fig. 8 Derived methodology for using the electrode displacement



The subsequent detection of weld spatter with the aid of the indentation displacement in the weld time ( $\Delta s_w$ ) is trivial if a critical value is exceeded in the form of a yes/no decision, as shown in Fig. 9. The reason for this lies in the sudden loss of pressure from the molten nugget due to the ejected material, which enables the upper electrode to sink further into the material. This leads not only to a significantly higher indentation displacement in the weld time ( $\Delta s_w$ ), but also to a lower indentation displacement in the hold time ( $\Delta s_h$ ) (cf. Figure 3).

Figure 10 shows a spot weld with and without expulsion to emphasize the relevance of the indentation displacement. Both welds have been produced with F1-16-20-8-50-6 electrode tips,  $F_E = 4.5$  kN and the weld times shown in Table 2, while the weld without expulsion was made at the upper limit of the welding range ( $I_w = 7.9$  kA) and the weld with expulsion was made with an increased welding current of  $I_w = 9.0$  kA. It can be seen, that the resulting electrode indentation is increased by over 120% with expulsion due to the sudden loss of strength of the weld nugget during the process. This correlates to findings in the literature [20].

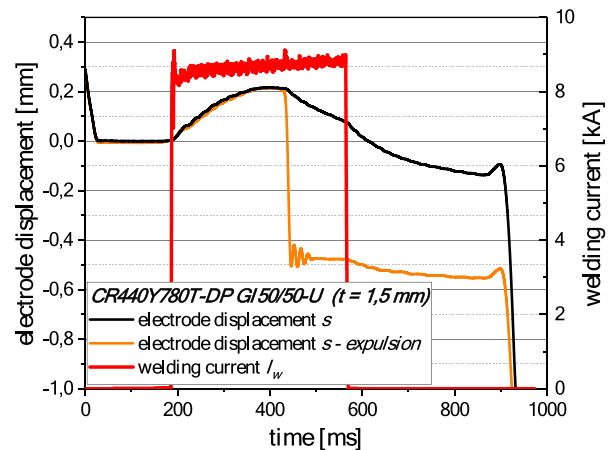
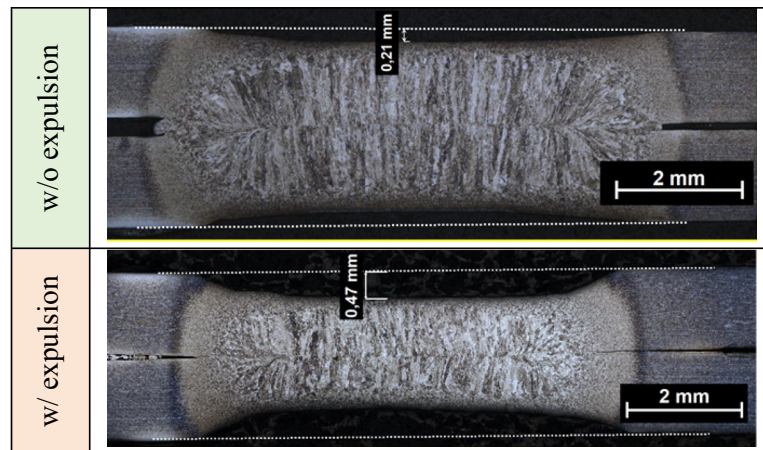


Fig. 9 Electrode displacement signal without (black) and with (orange) expulsion in the weld time

**Fig. 10** Spot weld for CR440Y780T-DP-GI50/50-U with and without expulsion



Furthermore, following Xia et al. [19], a linear correlation of the indentation displacement in the weld time with the mass loss caused by the expulsion could be determined (cf. Figure 5). This observation, combined with the finding that the indentation displacement in the weld time undergoes a correspondingly high change when the welding current is increased, leads to the proposed use of the parameter for expulsion evaluation.

The changes on the indentation displacement within the weld and hold time as a function of the spot diameter are illustrated in Fig. 5 and Fig. 11. Here, the ideal condition without a manufacturing discontinuity is displayed. An electrode force of  $F_E = 4.5$  kN with electrode tips F1-16-20-8-50-6 (cf. Table 2) with varying welding currents was used.

Figure 5 and Fig. 11 illustrate the use of the indentation displacement in the hold time ( $\Delta s_h$ ) to ensure that the minimum spot diameter ( $d_{wmin}$ ) has been reached. Here, a

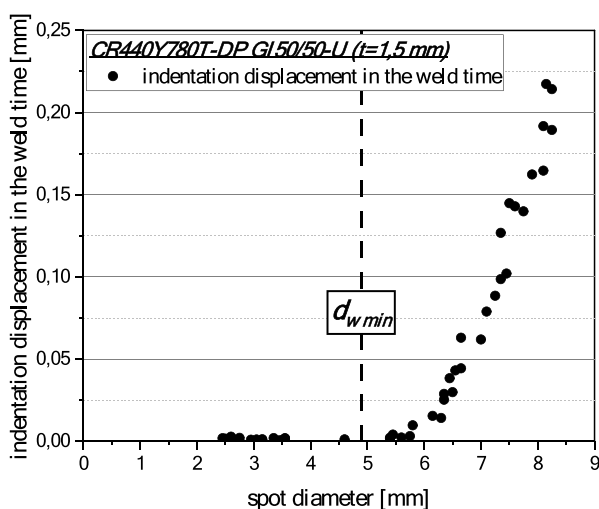


**Fig. 11** Indentation displacement in the weld time under ideal conditions

considerable change of the indentation displacement in the holding time is shown, especially for small spot diameters, so that a limit can be derived. In the experiments shown for the CR440Y780T-DP GI50/50-U, this limit value for achieving the minimum spot diameter ( $d_{wmin} = 4.90$  mm) is  $\Delta s_h \approx 0.16$  mm. Furthermore, the determined limit value proved to be robust against occurring disturbance variables, so that it can be used for the prediction of a minimum spot diameter (cf. Figure 6). The indentation displacement in the hold time significantly correlates to the nugget diameter due to the fact that the distance the electrodes sink into the material is expected to depend strongly on the amount of molten material at the end of the welding process. The more molten material is present when the current is shut off, the further the electrodes can sink in, which leads to the conclusion that a higher nugget diameter has been achieved. The use of the indentation displacement in the hold time also comes with the advantage that it is independent of the amount of welding pulses in comparison to the indentation displacement in the weld time. A variation of the holding times and its influence on the reliability of the results will be verified in further experiments.

In addition to that stiffness analysis will be carried out in order to calculate an appropriate correction factor for the electrode displacement on different welding machines.

## 5 Conclusions

A methodology for evaluating a resistance spot welding process based on the electrode displacement has been derived from the welding tests and data evaluations carried out with a galvanized dual-phase steel CR440Y780T-DP GI50/50-U ( $t = 1.5$  mm). The methodology is split into three steps, consisting of the following:



- (1) The detection of the presence of a discontinuity by means of the average nugget growth velocity in the first half of the spot weld process
- (2) The detection and evaluation of weld expulsion based on the indentation displacement within the weld time ( $\Delta s_w$ )
- (3) The evaluation of the achieved spot diameter based on the indentation displacement in the hold time ( $\Delta s_h$ )

It was shown that it is possible to evaluate a resistance spot welding process based on the proposed procedure. The methodology proved to be particularly sensitive for the detection of an angular misalignment. Further discontinuities, including axial misalignment, larger gaps, and severe electrode degradation will be investigated in future investigations. It is expected that the axial misalignment will have a similar effect like the angular misalignment, with the severity influencing the offset in the displacement curve. It is also expected that the electrode degradation has a significant influence on the electrode displacement, as it changes both the heat input and the contact area.

In further experiments, the methodology will also be validated using a multi-pulse welding process and adapted for the evaluation of other materials and multi-sheet joints. Furthermore, a parameterization of a resistance spot welding process based on the presented characteristics as well as mechanical tests in the form of shear and cross tension tests will be carried out.

**Acknowledgements** The authors would like to thank AiF for funding the IGF-Project IGF-No. 20.841 BR of the German Federation of Industrial Research Association (AiF), which was part of the program to support cooperative industrial research (Industrielle Gemeinschaftsförderung (IGF)) by the Federal Ministry for Economic Affairs and Energy, following a decision of the German Bundestag. Equal thanks go to all companies, colleagues, and students who contributed their support, knowledge, and effort to the project.

**Funding** Open Access funding enabled and organized by Projekt DEAL. This research was funded by the Research Association on Welding and Allied Processes of the DVS, part of the program to support cooperative industrial research (IGF) by the Federal Ministry for Economic Affairs and Energy, grant number IGF-Nr.: 20.841 BR (DVS-Nr.: 04.3193).

**Data availability** The underlying data of the shown results is available from the corresponding author, moritz.ullrich@ovgu.de, upon request.

## Declarations

**Competing interests** The authors declare no competing interests.

**Open Access** This article is licensed under a Creative Commons Attribution 4.0 International License, which permits use, sharing, adaptation, distribution and reproduction in any medium or format, as long as you give appropriate credit to the original author(s) and the source, provide a link to the Creative Commons licence, and indicate if changes were made. The images or other third party material in this article are included in the article's Creative Commons licence, unless indicated

otherwise in a credit line to the material. If material is not included in the article's Creative Commons licence and your intended use is not permitted by statutory regulation or exceeds the permitted use, you will need to obtain permission directly from the copyright holder. To view a copy of this licence, visit <http://creativecommons.org/licenses/by/4.0/>.

## References

1. Wohner M, Mitzschke N, Jüttner S (2021) Resistance spot welding with variable electrode force—development and benefit of a force profile to extend the weldability of 22MnB5+AS150. *Weld World* 65:105–117. <https://doi.org/10.1007/s40194-020-01001-2>
2. Zhang H (2011) Resistance welding: fundamentals and applications, Second Edition, 2nd edn. CRC Press, Hoboken
3. Nee AYC (ed) (2015) Handbook of manufacturing engineering and technology. Springer Reference, London
4. Gedeon SA, Eagar TW (1986) Resistance spot welding of galvanized steel: part II. Mechanisms of spot weld nugget formation. *Metall Mater Trans B* 17:887–901. <https://doi.org/10.1007/BF02657152>
5. Ighodaro OL-R, Biro E, Zhou YN (2017) Study and applications of dynamic resistance profiles during resistance spot welding of coated hot-stamping steels. *Metall and Mat Trans A* 48:745–758. <https://doi.org/10.1007/s11661-016-3899-3>
6. Xia Y-J, Lv T-L, Li Y-B et al (2023) Quantitative interpretation of dynamic resistance signal in resistance spot welding. *Weld J* 102:69–87
7. Lee J, Noh I, Jeong SI et al (2020) Development of real-time diagnosis framework for angular misalignment of robot spot-welding system based on machine learning. *Proc Manuf* 48:1009–1019. <https://doi.org/10.1016/j.promfg.2020.05.140>
8. ASM International (ed) (2012) Resistance spot welding of dual-phase steels: Heat affected zone softening and tensile properties, Proceedings of the 9th International Conference
9. Roy TK, Bhattacharya B, Ghosh C et al (eds) (2018) Advanced high strength steel: processing and applications. SpringerLink Bücher. Springer Singapore, Singapore
10. Lin HC, Hsu CA, Lee CS et al (2018) Effects of zinc layer thickness on resistance spot welding of galvanized mild steel. *J Mater Process Technol* 251:205–213. <https://doi.org/10.1016/j.jmatprot.2017.08.035>
11. Tumuluru M (2007) The effect of coatings on the resistance the effect of coatings on the resistance spot welding behavior of 780 MPa dual-phase steel: both the hot-dipped galvanized and the galvanized steels exhibited similar welding behavior. *Weld J* 86:161–169
12. Razmpoosh MH, DiGiovanni C, Zhou YN et al (2021) Pathway to understand liquid metal embrittlement (LME) in Fe-Zn couple: from fundamentals toward application. *Prog Mater Sci* 121:100798. <https://doi.org/10.1016/j.pmatsci.2021.100798>
13. Pant P, Hilpert B, Schubert H et al (2023) Liquid metal embrittlement behavior of dual-phase steels: the influence of microstructure and strain rate. TMS 2023 152nd annual meeting & exhibition supplemental proceedings. Springer Nature Switzerland, Cham, pp 973–983
14. Zhang P, Zhang H, Chen J et al (2007) Quality monitoring of resistance spot welding based on electrode displacement characteristics analysis. *Front Mech Eng China* 2:330–335. <https://doi.org/10.1007/s11465-007-0058-y>
15. American Welding Society (2022) Test methods for evaluating the resistance spot welding behavior of automotive sheet steel materials, 4th edn. American Welding Society, Miami, FL

16. Stahlinstitut VDEh Prüf- und Dokumentationsrichtlinie für die Fügeignung von Feinblechen aus Stahl - Teil 2: Widerstandspunktschweißen: Teil 2: Widerstandspunktschweißen(SEP 1220–2:2011–08)
17. Farson DF, Chen JZ, Ely et al (2004) Monitoring resistance spot nugget size by electrode displacement. *J Manuf Sci Eng* 126:391–394. <https://doi.org/10.1115/1.1644550>
18. Xia Y-J, Zhou L, Shen Y et al (2021) Online measurement of weld penetration in robotic resistance spot welding using electrode displacement signals. *Measurement* 168:108397. <https://doi.org/10.1016/j.measurement.2020.108397>
19. Xia Y-J, Shen Y, Zhou L et al (2021) Expulsion intensity monitoring and modeling in resistance spot welding based on electrode displacement signals. *J Manuf Sci Eng* 143:031008. <https://doi.org/10.1115/1.4048441>
20. Song S, Shojaee M, Midawi A et al (2023) Influence of expulsion and heat extraction resulting from changes to electrode force on liquid metal embrittlement during resistance spot welding. *J Market Res* 23:1458–1470. <https://doi.org/10.1016/j.jmrt.2023.01.093>

**Publisher's Note** Springer Nature remains neutral with regard to jurisdictional claims in published maps and institutional affiliations.